Analysis of reaction dynamics considering MAD by Langevin equation

Yoshihiro Aritomo[1,*], *Shota* Amano[1], *Shinya* Takagi[1], and *Masahisa* Ohta[2]

[1]Faculty of Science and Engineering, Kindai University, Osaka, Japan
[2]Konan University, Kobe, Japan

Abstract. In heavy ion fusion and nucleon transfer reactions, which lead to the synthesis of superheavy elements, it is important to understand the reaction mechanisms. The fusion reaction mechanism is analyzed in the case of deformed target nuclei such as actinide target nuclei. We have analyzed the correlation between fission fragment mass and scattering angle (MAD) using the Langevin equation. Taking into account the effect of the collision direction between the projectile and deformed target nuclei, we present the analysis of the experimental data for the MAD of ^{32}S+^{232}Th.

1 Introduction

The theoretical calculations predicted the existence of stable nuclei in the superheavy elemental region centered on 114 protons and 184 neutrons as "Island of Stability" in the 1960s. Since then, experimental studies using heavy-ion fusion reactions with large accelerators have been actively conducted mainly in the United States, Russia (former Soviet Union), and Germany, aiming at Island of Stability. With the synthesis of new elements, the number of elements on the periodic table has increased one by one. Recently, RIKEN in Japan succeeded in synthesizing element 113 and named the element nihonium (Nh), leaving its result on the periodic table. Currently, the atomic number has been named up to 118 (oganesson, Og), and the impact of the synthesis of new elements has been very high along with new element names [1–8].

Although heavy-ion fusion reactions have been conventionally used to produce such unknown heavy nuclei, the methods based on multi nucleon transfer reactions (MNT) have recently been attracting renewed attention, which were widely used in the 1970s and 1980s. The usefulness of MNT reactions for the studies in unexplored areas on the nuclear chart (unknown neutron-rich heavy and superheavy nuclei) has been discussed [9–17]. Recently, the advantage of MNT reactions in producing neutron-rich nuclei ($N = 126$) in contrast to fragmentation reactions [18–20] was revealed [21].

The whole reaction process in the superheavy element region is very complicated. They are divided into reaction processes, fusion-fission (FF), quasi-fission (QF), and deep-inelastic collision (DIC) process, and the probability of forming compound nuclei (CN) is extremely small. The mechanisms of these reactions have not been elucidated in detail, and various experimental techniques have been treid to clarify the reaction mechanisms. One of these methods is the use of a correlation between fission fragment mass and scattering angle is also important for understanding the reaction dynamics of fusion (MAD) [22–28]. This has been experimentally measured by a research group at the Australian National University (ANU). Theoretical studies to analyze MAD have been performed by a group at ANU using microscopic models such as TDHF. However, not many computational methods using the Langevin equation have been used to analyze MAD.

Studies of MAD using the Langevin equation with spherical nuclei as target nuclei have been conducted, and experimental data have been reproduced and analyzed [29, 30]. However, in studies using deformed nuclei as target nuclei, it has not been reproduced the experimental data. In this study, we try to calculate and analyze the MAD when deformed nuclei are used as target nuclei. We investigate the reaction system of ^{32}S + ^{232}Th, that the ^{232}Th nucleus is deformed and ^{32}S nucleus is spherical.

In the following section, the Langevin-type approach taking into account the orientation effects is described. The nuclear orientation effects for the mass drift in the ^{32}S + ^{232}Th reaction is followed in Sec. 3, where the mass drift and the MAD are discussed in detail and the summary is noted in the final section.

2 Theoretical framework

2.1 Transition to the adiabatic state

We adopt the dynamical model based on the multidimensional Langevin equations [31]. Potential energy changes gradually from diabatic potential to adiabatic potential with reaction time [13–16, 32, 33, 41].

Therefore, we treat the transition of two reaction stages with a time-dependent weighting function:

$$V = V_{\rm diab}(q) f(t) + V_{\rm adiab}(q)[1 - f(t)], \quad (1)$$

$$f(t) = \exp\left(-\frac{t}{\tau_{\rm DA}}\right). \quad (2)$$

*e-mail: aritomo@emat.kindai.ac.jp

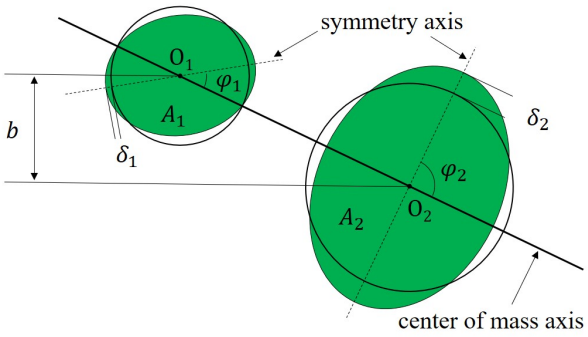

Figure 1. Geometrical diagram when both the deformed incident nucleus and the target nucleus collide with each other in the different initial orientation angles.

Here, q denotes a set of collective coordinates representing nuclear shape. The diabatic potential $V_{\rm diab}(q)$ is calculated within the double-folding method with Migdal nucleon-nucleon forces [31–34]. The adiabatic potential energy $V_{\rm adiab}(q)$ of the system is calculated using an extended two-center shell model [33]. The interaction time t used here is the time starting with the contact time between the projectile and target nuclei as zero. $f(t)$ is the weighting function included the relaxation time $\tau_{\rm DA}$. We use the relaxation time $\tau_{\rm DA} = 0.1$ zs proposed in [35–37]. With the two-center parameterizations [38, 39], the nuclear shape is represents by three deformation parameter is defined as follows: z_0 (distance between the centers of two potentials), δ (deformation of fragment), and α (mass asymmetry of colliding nuclei); $\alpha = \frac{A_2-A_1}{A_2+A_1}$, where A_1 and A_2 not only stand for the mass numbers of the projectile and target respectively [32, 40] but also are then used to indicate mass numbers of the two fission (light and heavy) fragments. The parameter δ is defined as $\delta = \frac{3(a-b)}{(2a+b)}$, where a and b represent the half length of the ellipse axes in the z_0 and ρ directions, respectively [38]. In addition, we use scaling to save computation time and use the coordinate z defined as $z = \frac{z_0}{(R_{\rm CN}B)}$, where $R_{\rm CN}$ denotes the radius of the spherical compound nucleus and the parameter B is defined as $B = \frac{(3+\delta)}{(3-2\delta)}$. We solve the dynamical equation numerically. Therefore, we restricted the number of degrees of freedom as three deformation parameters to avoid the huge calculation time.

2.2 Consideration of the nuclear orientation

When we use the deformed nucleus, in order to consider the orientation effects we apply the axially-symmetric potential $V_{\rm ax}^{\rm sym}$ the axially-asymmetric one $V_{\rm ax}^{\rm asym}$ in the stage of the diabatic potential. When two deformed nuclei collide with each other, mainly there are four colliding patterns: the so-called tip-to-tip ($\varphi_1^0 = \varphi_2^0 = 0$), side-to-side ($\varphi_1^0 = \pi/2, \varphi_2^0 = \pi/2$), tip-to-side ($\varphi_1^0 = 0, \varphi_2^0 = \pi/2$) and side-to-tip ($\varphi_1^0 = \pi/2, \varphi_2^0 = 0$). φ_1^0 and φ_2^0 denote the initial orientation angle of the projectile and target nuclei corresponding to φ_1 and φ_2 shown in Fig. 1. Here, we investigae the reaction system of ^{32}S + ^{232}Th. We select the various φ_2^0 of the deformed ^{232}Th nucleus fixing $\varphi_1^0 = 0$ of the spherical ^{32}S nucleus. In the treatment of the spherical nucleus ^{32}S, it makes sense to define angles even for spherical nuclei, since the model used now is treated as a classical system.

In the case of the tip collision ($\varphi_2^0 = 0$), we use the diabatic potential of axially-symmetric states $V_{\rm diab} = V_{\rm ax}^{\rm sym}$. If calculations for the side collision ($\varphi_2^0 = \pi/2$) or colliding patterns of the others ($0 < \varphi_2^0 < \pi/2$) are performed, we use the diabatic potential of axially-asymmetric states $V_{\rm diab} = V_{\rm ax}^{\rm asym}$. Here, note that $V_{\rm ax}^{\rm asym}$ depends on the nuclear orientation angle. Besides, while $V_{\rm diab}$ of the axially-asymmetric states transits to $V_{\rm adiab}$ which is the axially-symmetric states, the ellipsoid deformations are adjusted with restores of the systems using the time-dependent form, and the final ellipsoid deformations $\delta_i^{\rm fin}$ [41] finished the restoration of the axially-symmetry is obtained as

$$\tilde{\delta} = \delta_i f_{\rm res}(t) + \delta_i^{\rm fin}\left[1 - f_{\rm res}(t)\right], \tag{3}$$

$$f_{\rm res}(t) = \exp\left(-\frac{t}{\tau_{\rm res}}\right), \tag{4}$$

$$\delta_i^{\rm fin} = (1+\delta_i)\left[\delta_i(2+\delta_i)\sin^2\varphi_i^0 + 1\right]^{-\frac{3}{4}} - 1. \tag{5}$$

$f_{\rm res}$ is the weighting function including the relaxation time $\tau_{\rm res}$, which performs the restoration from the axially-asymmetric system to the axially-symmetric one. We use $\tau_{\rm res} = 1$ zs in this paper. This value involved in the restoration of the system is also has been used in Ref. [41]. In the collision system using the deformed ^{232}Th nucleus, we treat as $\delta_i \sim 0.18$ with $\delta_i = 3\beta_2/(\beta_2 + \sqrt{16\pi/5})$ [42]. The quadrupole deformation β_2 for the deformed nucleus ^{232}Th is 0.207 [43]. The details of the calculation method are described in the Ref. [44]

2.3 Dynamical equations

The trajectory calculations are performed on the time-dependent potential energy [31, 32, 40] using the multi-dimensional Langevin-type equations [32, 40, 45] as fol-

lows:

$$\frac{dq_i}{dt} = \left(m^{-1}\right)_{ij} p_j, \tag{6}$$

$$\frac{dp_i}{dt} = -\frac{\partial V}{\partial q_i} - \frac{1}{2}\frac{\partial}{\partial q_i}\left(m^{-1}\right)_{jk} p_j p_k - \gamma_{ij}\left(m^{-1}\right)_{jk} p_k + g_{ij}\Gamma_j(t), \tag{7}$$

$$\frac{d\vartheta}{dt} = \frac{\hbar L}{\Im}, \tag{8}$$

$$\frac{d\varphi_1}{dt} = \frac{\hbar L_1}{\Im_1}, \tag{9}$$

$$\frac{d\varphi_2}{dt} = \frac{\hbar L_2}{\Im_2}, \tag{10}$$

$$\frac{dL}{dt} = -\frac{1}{\hbar}\frac{\partial V}{\partial \theta} - \gamma_{\tan}\left(\frac{L}{\mu_R R^2} - \frac{L_1}{\Im_1}a_1 - \frac{L_2}{\Im_2}a_2\right)R + \frac{R}{\hbar}\sqrt{\gamma_{\tan}T}\Gamma_{\tan}(t), \tag{11}$$

$$\frac{dL_1}{dt} = -\frac{1}{\hbar}\frac{\partial V}{\partial \varphi_1} + \gamma_{\tan}\left(\frac{L}{\mu_R R^2} - \frac{L_1}{\Im_1}a_1 - \frac{L_2}{\Im_2}a_2\right)a_1 - \frac{a_1}{\hbar}\sqrt{\gamma_{\tan}T}\Gamma_{\tan}(t), \tag{12}$$

$$\frac{dL_2}{dt} = -\frac{1}{\hbar}\frac{\partial V}{\partial \varphi_2} + \gamma_{\tan}\left(\frac{L}{\mu_R R^2} - \frac{L_1}{\Im_1}a_1 - \frac{L_2}{\Im_2}a_2\right)a_2 - \frac{a_2}{\hbar}\sqrt{\gamma_{\tan}T}\Gamma_{\tan}(t). \tag{13}$$

The collective coordinates q_i represent z, δ, and α, the symbol p_i denotes momentum conjugated to q_i, and V is the multidimensional potential energy. m_{ij} and γ_{ij} stand for the shape-dependent collective inertia and friction tensors, respectively. We adopted the hydrodynamical inertia tensor m_{ij} in the Werner-Wheeler approximation for the velocity field [45]. The one-body friction tensors γ_{ij} are evaluated within the wall-and-window formula [46, 47]. The normalized random force $\Gamma_i(t)$ is assumed to be white noise: $\langle\Gamma_i(t)\rangle = 0$ and $\langle\Gamma_i(t_1)\Gamma_j(t_2)\rangle = 2\delta_{ij}\delta(t_1 - t_2)$. According to the Einstein relation, the strength of the random force g_{ij} is given as $\gamma_{ij}T = \sum_k g_{ik}g_{jk}$. ϑ and μ_R indicate the relative orientation of nuclei and the reduced mass. R is the distance between the nuclear centers O_1O_2 as shown in Fig. 1. φ_1 and φ_2 stand for the orientation angles of each nucleus (See Fig. 1). $a_{1,2} = \frac{R}{2} \pm \frac{R_1 - R_2}{2}$ is the distance from the center of the fragment to the middle point between the nuclear surfaces, and $R_{1,2}$ is the nuclear radii. Here, $\Im$ and L represent the moment of inertia of the rigid body with deformation q and the relative orientation of nuclei and relative angular momentum respectively. The moment of inertia and the angular momentum for the heavy and light fragments are $\Im_{1,2}$ and $L_{1,2}$, respectively. The total angular momentum $L_{\rm tot} = L + L_1 + L_2$ is preserved. The phenomenological nuclear friction forces for separated nuclei are expressed in terms of the tangential friction $\gamma_{\tan}$ and the radial friction γ_R using the Woods-Saxon radial form factor suggested in Ref. [32]. The treatment of $\gamma_{\tan}$ and γ_R are described in our previous papers [48, 49].

2.4 Mass ratio $M_{\rm R}$ and scattering angle $\theta_{\rm c.m.}$

The MAD is presented by the mass-angle matrix using $M_{\rm R}$ and the scattering angle $\theta_{\rm c.m.}$. The projectile-like mass ratio $M_{\rm R}$ is determined as $M_R = A_1/A_{\rm CN}$. Consequently, the target-like mass ratio is expressed as $M_R = 1 - M_R$. Regarding the scattering angle $\theta_{\rm c.m.}$ is determined as Ref. [44].

3 RESULTS AND DISCUSSION

The hot fusion reaction, one of the experimental methods in the synthesis of superheavy elements, uses actinide nuclei as target nuclei and has so far succeeded in the synthesis of element 118. The actinide nuclei used in the hot fusion reaction are deformed one, and the role of this deformation effect is significant in fusion process. A mechanism that increases the fusion probability by side collision has been reported, and such an effect is thought to have led to the successful synthesis of the new element.

It is therefore very important to analyze in detail the effects of deformed target nuclei in the fusion process. In a previous study, the mass distribution of fission fragments and the capture, fusion and evaporation residue cross-sections were measured in the S+U and Si+U reactions by the JAEA group [50, 51]. Experimental data on MAD targeting deformed nuclei by ANU have been reported [52]. However, in our previous study [29, 30], theoretical calculations using Langevin failed to reproduce the trend of the experimental MAD, because we did not consider the orientation effects. In this paper, we present the results of calculations with deformed nuclei as target, using the model described in Section 2.

In the following, the effect on our calculation taking account of the orientation of the deformed target in the collision of ^{32}S + ^{232}Th at $E_{\rm c.m.}/V_{\rm bass} = 1.108$ is presented. Here, the Bass barrier energy $V_{\rm bass}$ in the ^{32}S + ^{232}Th is 158.55 MeV [52]. The calculations are performed in the range $0.15 < {\rm M_R} < 0.85$ (to simply eliminate quasielastic events).

Figure 2 shows the MADs of ^{32}S + ^{232}Th at $E_{\rm c.m.}/V_{\rm bass} = 1.108$ in seven orientation angles of the deformed ^{232}Th nucleus. In Fig. 2(a), we can see that the mass-asymmetric fission is dominant and the mass evolution is restricted to producing fragments with $M_R = 0.3, 0.7$.

This restriction in the mass evolution is due to the narrow neck cross-sectional area rather, because the interaction energy is enough high above the barrier. The projectile and the target nucleus stick together in more than a half rotation, and as the orientation angle of ^{232}Th becomes large, the mass equilibration progresses in the meantime. In contrast with the tip collision case, although the MAD for the side collision (See Fig. 2(g)) is dominated by the mass-symmetric fission, a significant correlation between mass and angle can still be seen. This result implies that QF events are dominant even for the side collision case. Namely, even if the mass-symmetric fission events are dominant, many of their trajectories do not path through the compound nucleus area.

The integrated MAD and $M_{\rm R}$ distribution over the nuclear orientations of the deformed nucleus ^{232}Th are shown in Fig. 3. A strong correlation between mass and angle

can be seen in Fig. 3(a). The experimental trend [52] is reproduced in Fig. 3(a). Figure 3(b) shows MAD projected onto the M_R axis and the solid curve which gives a good agreement with the experimental trend [54]. The experimental results are inferred to be a mix of fission products in all nuclear orientation angles because the incident energy is sufficiently high. The calculations were made for all orienation angles as initial conditions, and the results (as shown in Fig. 2) were added together to produce the Fig. 3(b), which were composited with the same weights for each angle. More quantitative analysis of M_R is a future task.

4 Summary

We have performed the model calculation for the MAD and M_R considering the orientations of the target nucleus. The variation of the mass evolution and the rotation angle of fragments have clarified changing the orientation of the target nucleus from 0° (the tip collision) to 90° (the side collision). The integrated MAD and M_R distribution over the nuclear orientations are in good agreement with the feature of the experimental results. However, further investigations are needed for more precise reproduction of the experimental M_R. More importantly, the strong mass-angle correlation was also reproduced. It is found that the fusion probability for the side collision is highest for any orbital angular momentum.

The Langevin calculation were performed using the cluster computer system (Kindai-VOSTOK) which is supported by JSPS KAKENHI Grant Number 20K04003 and Research funds for External Fund Introduction 2021 by Kindai University.

References

[1] Y. T. Oganessian and K. P. Rykaczewski, Phys. Today **68**, 32.
[2] S. Hofmann and G. Münzenberg, Rev. Mod. Phys. **72**, 733 (2000).
[3] Yu. Ts. Oganessian, V. K. Utyonkov, Yu. V. Lobanov, F. Sh. Abdullin, A. N. Polyakov, R. N. Sagaidak et al., Phys. Rev. C **74**, 044602 (2006).
[4] S. Hofmann, D. Ackermann, S. Antalic, H. G. Burkhard, V. F. Comas, R. Dressler et al., Eur. Phys. J. A **32**, 251 (2007).
[5] S. Hofmann, V. Ninov, F. P. Heßberger, P. Armbruster, H. Folger, G. Münzenberg et al., Z. Phys. A: Hadrons Nucl. **350**, 277 (1995).
[6] P. Armbruster, Annu. Rev. Nucl. Part. Sci. **35**, 135 (1985).
[7] G. Munzenberg, Rep. Prog. Phys. **51**, 57 (1988).
[8] K. Morita, K. Morimoto, D. Kaji, T. Akiyama, S.-i. Goto, H. Haba et al. , J. Phys. Soc. Jpn. **76**, 043201 (2007).
[9] P.-H. Chen, F. Niu, W. Zuo, and Z.-Q. Feng, Phys. Rev. C **101**, 024610 (2020).
[10] L. Zhu, J. Su, C. Li, and F.-S. Zhang, Phys. Lett. B **829**, 137113 (2022).
[11] L. Zhu, Chin. Phys. C **43**, 124103 (2019).
[12] S. Heinz and H. Devaraja, Eur. Phys. J. A **58**, 114 (2022).
[13] V. I. Zagrebaev and W. Greiner, Phys. Rev. C **83**, 044618 (2011).
[14] V. Zagrebaev and W. Greiner, J. Phys. G: Nucl. Part. Phys. **35**, 125103 (2008).
[15] V. Zagrebaev, A. Karpov, and W. Greiner, J. Phys: Conf. Seri. **420**, 012001 (2013).
[16] V. I. Zagrebaev and W. Greiner, Phys. Rev. C **87**, 034608 (2013).
[17] V. Zagrebaev and W. Greiner, Phys. Rev. Lett. **101**, 122701 (2008).
[18] T. Kurtukian-Nieto, J. Benlliure, K.-H. Schmidt, L. Audouin, F. Becker, B. Blank et al., Phys. Rev. C **89**, 024616 (2014).
[19] J. Kurcewicz, F. Farinon, H. Geissel, S. Pietri, C. Nociforo, A. Prochazka et al., Phys. Lett. B **717**, 371 (2012).
[20] J. Taïeb, K.-H. Schmidt, L. Tassan-Got, P. Armbruster, J. Benlliure, M. Bernas et al., Nucl. Phys, A **724**, 413 (2003).
[21] Y. X. Watanabe, Y. H. Kim, S. C. Jeong, Y. Hirayama, N. Imai, H. Ishiyama et al., Phys. Rev. Lett. **115**, 172503 (2015). Phys. Rev. C **108**, 024602 (2023). Acta Phys. Polo. B **46** 427 (2015). Phys. Rev. C **101**, 014604 (2020). Phys. Rev. C **106**, 014606 (2022). Phys. Rev. Res.**5**, L022021 (2023). Phys. Rev. C **99**, 014613 (2019). Eur. Phys. J. A **58**, 41 (2022)
[22] J. Tōke, R. Bock, G. Dai, A. Gobbi, S. Gralla, K. Hildenbrand et al., Nucl. Phys. A **440**, 327 (1985).
[23] W. Q. Shen, J. Albinski, A. Gobbi, S. Gralla, K. D. Hildenbrand, N. Herrmann et al., Phys. Rev. C **36**, 115 (1987).
[24] R. du Rietz, E. Williams, D. J. Hinde, M. Dasgupta, M. Evers, C. J. Lin, D. H. Luong, C. Simenel, and A. Wakhle, Phys. Rev. C **88**, 054618 (2013).
[25] E. Prasad, A. Wakhle, D. J. Hinde, E. Williams, M. Dasgupta, M. Evers, D. H. Luong, G. Mohanto, C. Simenel, and K. Vo-Phuoc, Phys. Rev. C **93**, 024607 (2016).
[26] R. du Rietz, D. J. Hinde, M. Dasgupta, R. G. Thomas, L. R. Gasques, M. Evers, N. Lobanov, and A. Wakhle, Phys. Rev. Lett. **106**, 052701 (2011).
[27] T. Tanaka, D. J. Hinde, M. Dasgupta, E. Williams, K. Vo-Phuoc, C. Simenel et al., Phys. Rev. Lett. **127**, 222501 (2021).
[28] T. Tanaka, D. J. Hinde, M. Dasgupta, E. Williams, K. Vo-Phuoc, C. Simenel et al., Phys. Rev. C **107**, 054601 (2023).
[29] S. Amano, Y. Aritomo, S. Ishizaki, M. Okubayashi, and S. Okugawa, JAEA-Conf 2021-001, 102 (2022).
[30] S. Amano, Y. Aritomo, Y. Miyamoto, S. Ishizaki, and M. Okubayashi, Bulletin of the Russian Academy of Sciences: Physics, 84, 1034 (2020).
[31] V. Zagrebaev and W. Greiner, J. Phys. G: Nucl. Part. Phys. **34**, 2265 (2007).

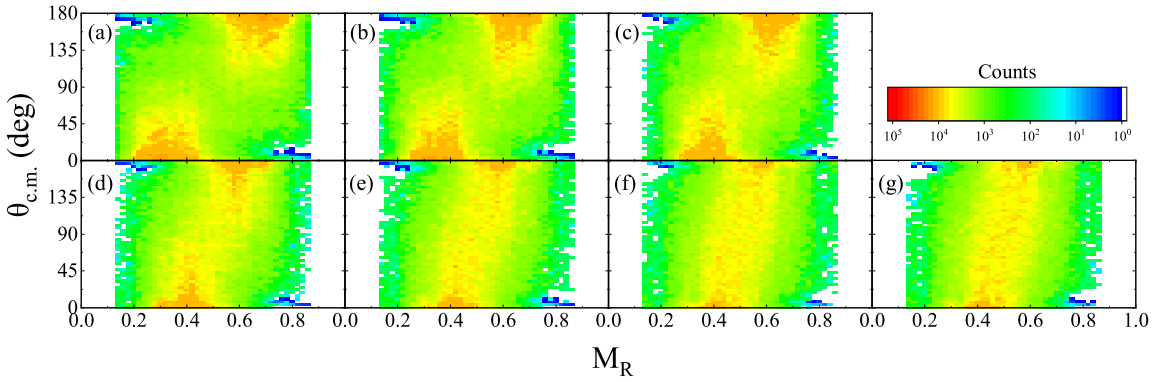

Figure 2. Seven panels (a) to (g) show calculated MADs for seven nuclear orientations (0°, 15°, 30°, 45°, 60°, 75°, 90°) of the deformed nucleus ^{232}Th. The calculation data are for the ^{32}S + ^{232}Th system at $E_{\mathrm{c.m.}}/V_{\mathrm{bass}}$ = 1.108. The MADs show a transition from mass-asymmetric associated with the orientation angle 0° (tip collision) to mass-symmetric associated with the orientation angle 90° (side collision).

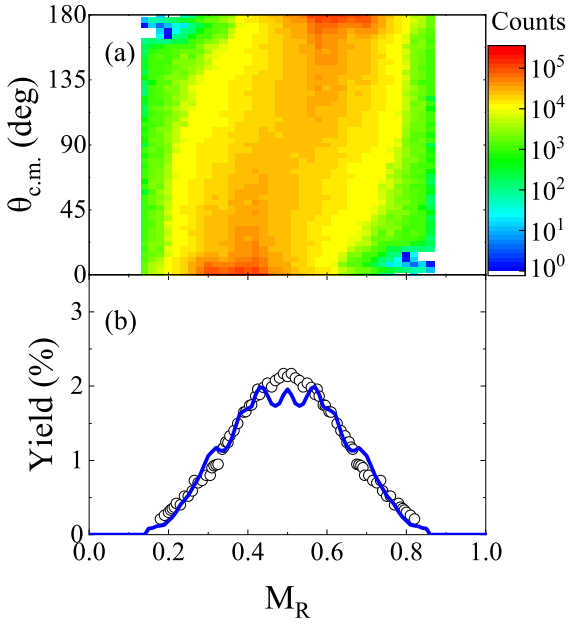

Figure 3. (a) Mass angle distribution and (b) M_{R} distribution calculated for ^{32}S + ^{232}Th at $E_{\mathrm{c.m.}}/V_{\mathrm{bass}}$ = 1.108. Calculations take into account the nuclear orientations of the deformed nucleus ^{232}Th. Open circles are the experimental data shown in [54]

[32] V. Zagrebaev and W. Greiner, J. Phys. G: Nucl. Part. Phys. **31**, 825 (2005).
[33] V. Zagrebaev, A. Karpov, Y. Aritomo, M. Naumenko, and W. Greiner, Phys. Part. Nucl. **38**, 469 (2007).
[34] A. B. Migdal, *Theory of Finite Fermi Systems and Applications to Atornic Nuclei* (Interscience Publishers, 1967).
[35] G. Bertsch, Z. Phys. A: Atom. nucl. **289**, 103 (1978).
[36] W. Cassing and W. Nörenberg, Nucl. Phys. A **401**, 467 (1983).
[37] A. Diaz-Torres, Phys. Rev. C **69**, 021603(R) (2004).
[38] J. Maruhn and W. Greiner, Z. Phys. **251**, 431 (1972).
[39] K. Sato et al., Z. Phys. A: Atom. nucl. **288**, 383 (1978).
[40] Y. Aritomo and M. Ohta, Nucl. Phys. A **744**, 3 (2004).
[41] V. V. Saiko and A. V. Karpov, Phys. Rev. C **99**, 014613 (2019).
[42] Y. Aritomo, K. Hagino, K. Nishio, and S. Chiba, Phys. Rev. C **85**, 044614 (2012).
[43] P. Moller, J. Nix, W. Myers, and W. Swiatecki, At. Data Nucl. Data Tables **59**, 185 (1995).
[44] S. Amano, Y. Aritomo, and M. Ohta, Y. Aritomo, Phys. Rev. C **80**, 064604 (2009).
[45] K. T. R. Davies, A. J. Sierk, and J. R. Nix, Phys. Rev. C **13**, 2385 (1976).
[46] J. Randrup and W. Swiatecki, Nucl. Phys. A **429**, 105 (1984).
[47] A. J. Sierk and J. R. Nix, Phys. Rev. C **21**, 982 (1980).
[48] S. Amano, Y. Aritomo, and M. Ohta, Phys. Rev. C **106**, 024610 (2022).
[49] S. Amano, Y. Aritomo, and M. Ohta, Phys. Rev. C **108**, 014612 (2023).
[50] K. Nishio, H. Ikezoe, S. Mitsuoka, I. Nishinaka, Y. Nagame, Y. Watanabe, T. Ohtsuki, K. Hirose, and S. Hofmann, Phys. Rev. **C 77**, 064607 (2008).
[51] K. Nishio, H. Ikezoe, I. Nishinaka, S. Mitsuoka, K. Hirose, T. Ohtsuki, Y. Watanabe, Y. Aritomo, and S. Hofmann, Phys. Rev. **C 82**, 044604 (2010).
[52] D. J. Hinde, R. du Rietz, M. Dasgupta, R.G. Thomas, L.R. Gasques, Phys. Rev. Lett. **101**, 092701 (2008).
[53] R. Bass, *Nuclear Reactions with Heavy Ions* (Springer, 1980).
[54] E. Galkina, E. Kozulin, G. Knyazheva, I. Itkis, A. Bogachev, I. Diatlov, et al., Bull. Russ. Acad. Sci.: Phys. **85**, 1085 (2021).